

Spin-orbit proximity effect in graphene on metallic substrates: decoration vs intercalation with metal adatoms

Jagoda Sławińska^{1,2,3} and Jorge I. Cerdá²

¹*Present address: Department of Physics, University of North Texas, Denton, TX 76203, USA*

²*Instituto de Ciencia de Materiales de Madrid, ICMN-CSIC, Cantoblanco, 28049 Madrid, Spain*

³*Department of Solid State Physics, University of Łódź, Pomorska 149/153, 90236 Łódź, Poland*
(Dated: July 10, 2019)

The so-called spin-orbit proximity effect experimentally realized in graphene (G) on several different heavy metal surfaces opens a new perspective to engineer the spin-orbit coupling (SOC) for new generation spintronics devices. Here, via large-scale density functional theory (DFT) calculations performed for two distinct graphene/metal models, G/Pt(111) and G/Au/Ni(111), we show that the spin-orbit splitting of the Dirac cones (DCs) in these structures might be enhanced by either adsorption of adatoms on top of graphene (decoration) or between the graphene and the metal (intercalation). While the decoration by inducing strong graphene-adatom interaction suppresses the linearity of the G's π bands, the intercalated structures reveal a weaker adatom-mediated graphene/substrate hybridization which preserves well-defined although broadened DCs. Remarkably, the intercalated G/Pt(111) structure exhibits splittings considerably larger than the defect-free case.

I. INTRODUCTION

Tuning of spin-orbit coupling (SOC) in graphene¹ is one of the fundamental steps to engineer graphene-based spintronics devices. One promising route to achieve this goal is the so-called spin-orbit proximity effect, recently extensively studied from both theoretical and experimental side.^{2–12} This mechanism of inducing SOC extrinsically relies on the proximity between graphene (G) and a metal; the SOC of the heavy atoms might be *transferred* to the G when both materials are brought sufficiently close to each other. Experimental realizations of spin-orbit proximity have revealed several important phenomena, such as spin Hall effect at room temperature shown by Avsar *et al.*² or even a more intriguing electron confinement associated to multiple topologically non-trivial gaps observed by Calleja *et al.* in graphene on Ir intercalated by Pb nanoislands (Pb/Ir).¹³

Recently, we have reported that the mechanism of inducing SOC in G when adsorbed on heavy metal surfaces is far more complex than it had been predicted before.¹⁰ DFT calculations of graphene on Pt(111) and on Au/Ni(111) showed that the induced spin texture is a result of spin-dependent hybridization between the Dirac cones (DCs) and the surface *d*-bands of the metal. The spin vector of graphene is determined by that of the substrate bands, and undertakes rotations wherever hybridization with any of the spin-orbit splitted metal bands occur. Consequently, the reported non-trivial spin textures, although intriguing from the fundamental point of view, seem difficult to control in any practical device. Furthermore, although hybridizations locally open mini-gaps around which the SOC-derived spin splitting may reach giant values above 100 meV, in the quasi-linear regions, where the G transport properties are most relevant, the splittings are typically of the order of just 10 meV.^{10,11}

The main purpose of this study is to theoretically ex-

plore alternative routes to increase the SOC derived splittings in the G by incorporating single metal adatoms at the graphene/metal interface. We consider two types of adsorption which should lead to two very different interaction scenarios: (i) decoration defined as the adsorption of the adatom on top of graphene and, (ii) intercalation of the adatom between the G and the metallic surface. The first case should induce changes mainly in the G's properties already perturbed by the metal surface, while the latter might significantly alter the graphene-substrate proximity, as graphene will now interact with the metal mainly via the intercalated adatom. Importantly, both decoration and intercalation can be realized experimentally^{12–23} and are known to provide several interesting options for engineering of graphene's properties, in addition to any possible enhancement of SOC.²⁴ Here, we will focus on two previously studied models, G/Pt(111) and G/Au/Ni(111) which present markedly different electronic and magnetic properties, and consider the adsorption of one species for each system, namely, a Pt adatom for G/Pt(111) and an Au adatom for G/Au/Ni(111).

The paper is organized as follows. In Sec II we provide a brief description of DFT calculations. Section III reports the electronic properties and spin textures of the G/Pt(111) calculated defect-free case and both types of adsorption. In Sec. IV we present a similar analysis for G/Au/Ni(111) structures. The conclusions are summarized in Sec. V.

II. METHODS

Our large-scale DFT calculations have been performed with the SIESTA code²⁵ as implemented within the GREEN package.^{26,27} The exchange-correlation (XC) potential has been treated using the generalized gradient approximation (GGA) in the Perdew, Burke, and Ern-

erhof formalism.²⁸ Dispersion forces were included via the semi-empirical scheme of Ortmann and Bechstedt.²⁹ Spin-orbit coupling has been self-consistently taken into account as implemented in Ref. 30. Core electrons have been simulated employing norm-conserving pseudopotentials of the Troulliers-Martin type, including core corrections for the metal atoms. The atomic orbital (AO) basis set based on double-zeta polarized strictly localized numerical orbitals has been generated employing a confinement energy of 100 meV. Real space three-center integrals have been computed over 3D-grids with a resolution equivalent to 500 Rydbergs mesh cut-off, while the Brillouin zone integrations have been performed over k -supercells of around (18×18) with respect to the G - (1×1) unit cell. The temperature kT in the Fermi-Dirac distribution has been set to 10 meV in all cases.

We have employed realistically large supercells to properly account for the the moiré patterns and reconstructions known for these systems as well as to minimize the direct interaction between the adatoms (Fig.1). In the case of the $G/Pt(111)$ we considered a thick $Pt(111)$ slab (6 layers) with graphene adsorbed on top assuming a G - $(3 \times 3)/Pt$ - $(\sqrt{7} \times \sqrt{7})R19.1^\circ$ supercell which corresponds to a minimal lattice mismatch.³¹ In order to reduce the interaction between defects among neighbouring supercells we have enlarged the (3×3) supercell to a (6×6) and placed a Pt adatom either on top of the G in an *atop* configuration (Pt_{ad}), or between the G and the Pt surface at an *fcc* site and below a C atom (Pt_{in}). On the other hand, we modeled the $G/Au/Ni(111)$ system assuming a $(9 \times 9)/(8 \times 8)/(9 \times 9)$ commensurability between the G , Au and Ni lattices, respectively, with the Au layer intercalated between the G and the four Ni layers thick slab. The Au adatoms have been incorporated either on top of the graphene at an *atop* site (Au_{ad}), or in between the G and the Au layer below a C atom and at an *hcp* site (Au_{in}). The final adsorption structures have been obtained after relaxing the graphene, the adatom, and the first two metal layers until forces were smaller than $0.04 \text{ eV}/\text{Å}$. In all calculations including SOC for the $G/Au/Ni(111)$ systems the spin quantization axis was set along the z direction (out-of-plane). Although estimates of the magnetic anisotropy employing the force theorem indicate that the in-plane magnetization is more favourable, we have chosen the out-of-plane orientation in order to preserve the $p3m$ symmetry and thus facilitate the interpretation of the spin textures. The effect of choosing a different spin quantization axis will be briefly discussed in section IV.

Finally, the electronic structures have been evaluated in the form of projected density of states $PDOS(\vec{k}, E)$ calculated for the semi-infinite surfaces constructed after replacing the bottom layers of the slabs by a semi-infinite bulk following the Green's functions based prescription detailed in Refs. 27 and 32. Unfortunately, unfolding the G -projected band structure into its primitive BZ is not possible in the adatom configurations since the strong interaction induce large distortions which break

the translation symmetry within the G layer. Hence, all projections are presented folded into the supercell's BZ.

III. $G/Pt(111)$: INTERCALATION VS DECORATION WITH Pt ADATOMS

Figure 1(a-c) shows the relaxed geometries of all considered $G/Pt(111)$ structures, that is; the defect-free case in (a), the intercalated adatom between G and the $Pt(111)$ surface in (b) and the atop adatom adsorption in (c). Figure 2 presents all the corresponding electronic structures and spin textures along the high-symmetry lines of the shrunk (6×6) BZ.

Let us first briefly summarize the main results obtained for the defect-free configuration as a detailed study for this case has already been presented in Ref. 10. Given the weak interaction indicated by the large G -metal distance of 3.37 Å (physisorption regime³³) the DCs can still be clearly resolved in the PDOS map in Fig. 2(a), where the G (red) and surface Pt (light blue) projections have been superimposed –recall that the G 's K and K' points are backfolded into the supercell's Γ point. In Figs. 2(b)-(c) we present the spin textures projected on the G and the Pt surface, respectively, where we have simultaneously plotted the three spatial components of the spin polarization employing a different color scheme for each of them: s_{\parallel} green, s_{\perp} red and s_z blue tones, where s_{\parallel} and s_{\perp} correspond to the in-plane spin components projected along the k -line and perpendicular to it, respectively, and s_z to the out-of-plane component. Contrary to the PDOS case, the G - Pt interaction can be clearly appreciated in these maps via the rich spin texture induced in the DCs by the hybridization with the d -bands, involving multiple spin reorientations in all the occupied states region and up to around 0.8 eV above the Fermi level (E_f). Furthermore, and as shown in Ref. 10, the splitting of the G bands is by no means uniform, attaining *giant* values larger than 100 meV at mini-gaps, but only a few tens of meV at most in the quasi-linear regions.

A. Intercalation between graphene and Pt surface

Intercalation of the Pt adatom (Pt_{in}) between the G and the substrate induces a strong buckling in the former with a corrugation as large as 0.8 Å , with short bond lengths of 2.1 Å between Pt_{in} and the closest carbon atoms. At the same time, the G layer is displaced upwards so that the lowest C atoms lie 3.7 Å above the Pt surface. In such geometry, we expect a weakening of the overall interaction of the G with the Pt surface at the expense of a stronger one with the intercalated defect. In the PDOS map presented in Fig. 2(a'), consisting of superimposed bands of G (red), Pt adatom (yellow) and the Pt surface (light blue), the adatom contribution appears as a rather faint smudge (yellowish tones) indicating, as expected, a strong hybridization with the continuum of

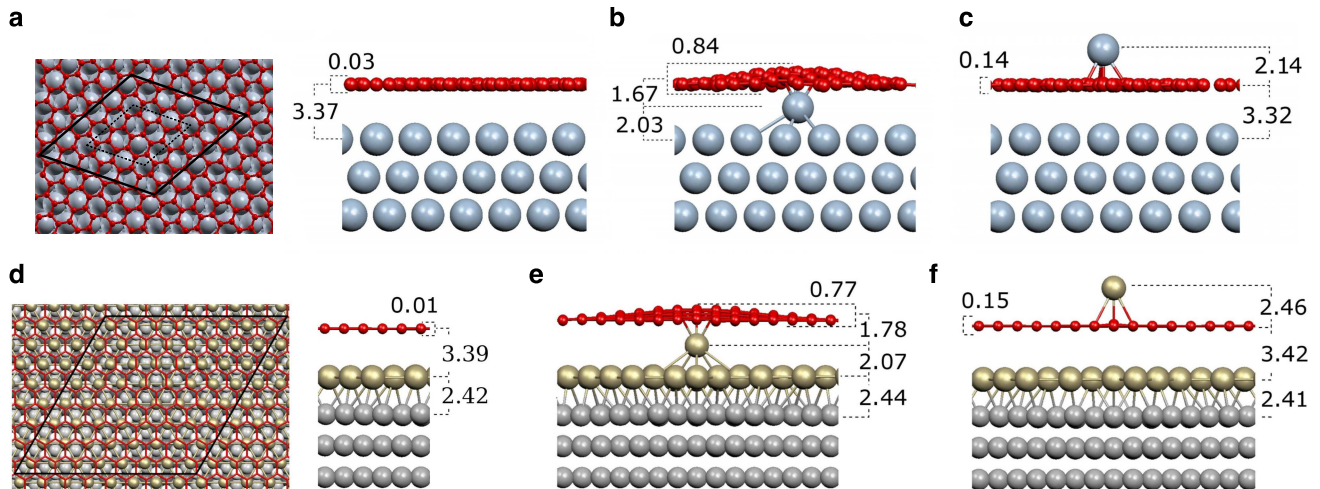


FIG. 1. (a) Top and side view of the G/Pt(111). The (3×3) supercell has been enlarged to (6×6) to avoid interactions between adatoms in configurations (b) and (c). (b) Side view of G/Pt(111) with Pt adatom intercalated between graphene and the first Pt layer. (c) Same as (b), but with Pt_{ad} placed above (on top) of a C atom in graphene. (d) Relaxed geometry of the G/Au/Ni(111) structure. (e) Same as (b) for G/Au/Ni(111). (f) Same as (c) for G/Au/Ni(111). Graphene is represented either by red balls or sticks, while Pt, Au and Ni atoms by blue, yellow and grey balls, respectively. The black parallelograms in (a) and (d) mark the $G(3 \times 3)/\text{Pt}(\sqrt{7} \times \sqrt{7})R19.1^\circ$ and $G(9 \times 9)/\text{Au}(8 \times 8)/\text{Ni}(9 \times 9)$ supercells, respectively. All distances are given in angstroms.

Pt bulk states. Close proximity of the C atoms with the Pt_{in} leads to important changes in the DCs with respect to the defect-free case; one of the cones vanishes almost entirely below E_f while the other remains well-preserved but strongly broadened in the whole considered region.

The G's spin structure, shown in panel (b'), also reveals strong differences with respect to the defect-free case. As can be inferred from the substrate's and adatom's spin textures shown in (c') and (d'), it now follows more closely the spin of the latter. In fact, due to the strong G- Pt_{in} interaction, the Dirac point can be clearly resolved in panel (d') as well as the strong hybridization with one of the DCs. Surprisingly, the Pt_{in} spin texture is markedly different from that at the Pt surface, which closely resembles the defect-free case (panel (c)), implying that the SOC at the surface is hardly affected by the presence of the adatom.

On the other hand, at energies above ~ 1 eV, there are hardly any Pt_{in} states and the DCs appear at first sight very similar as in the defect free case, allowing a direct comparison between their respective SOC induced splittings. Figure 3(b) presents single spectra corresponding to spin vector versus energy curves $\vec{s}(E)$ extracted from panel (b') for two selected k -points in the empty states region (indicated by white line segments). They are compared versus analogous data calculated for the defect-free model. The spin-splittings are clearly larger by at least a factor of two in the case of the intercalated model, although the PDOS (gray lines) is significantly broadened as a result of the strong G- Pt_{in} interaction. Thus, Pt_{in} intercalation appears as a quite efficient way to enhance

the spin-orbit proximity effect.

B. Pt adsorption on top of G/Pt(111)

Contrary to the intercalation case, the adsorption of a Pt adatom on top of G/Pt(111) leads to hardly any buckling of the G with a corrugation below 0.1 Å (see Fig. 1). However, a very short distance between the adatom and the G (2.14 Å) induces a strong interaction and important changes in the G's electronic structure, as can be noticed in Fig. 2 (a'') where the PDOS(\vec{k}, E) of G, Pt_{ad} and Pt(111) are superimposed following the same color scheme as in (a'). The most striking feature is the bunch of intense localized bands belonging to the adatom (yellow) which completely tear the lower DCs and notably alter the upper ones. Such picture is consistent with a simpler model where the Pt surface has been removed. Indeed, the PDOS of a pure G+ Pt_{ad} configuration, shown in Fig. 8(a) in the Appendix A, strongly resembles the one in panel (a''), indicating that the G- Pt_{ad} interaction overrules that with the Pt substrate as expected from their close proximity. An orbital analysis of the adatom's states reveals that below E_f all of them are mainly of $5d$ character, while only the band at approximately $+400$ meV, which crosses the Dirac point, has an sp origin.

The same applies to the spin textures shown in Figs. 2(b''-d''). The G and Pt_{ad} projections (panels (b'') and (d'')), respectively) are highly reminiscent of their substrate-free counterparts in Fig. 8(b) and (c). The

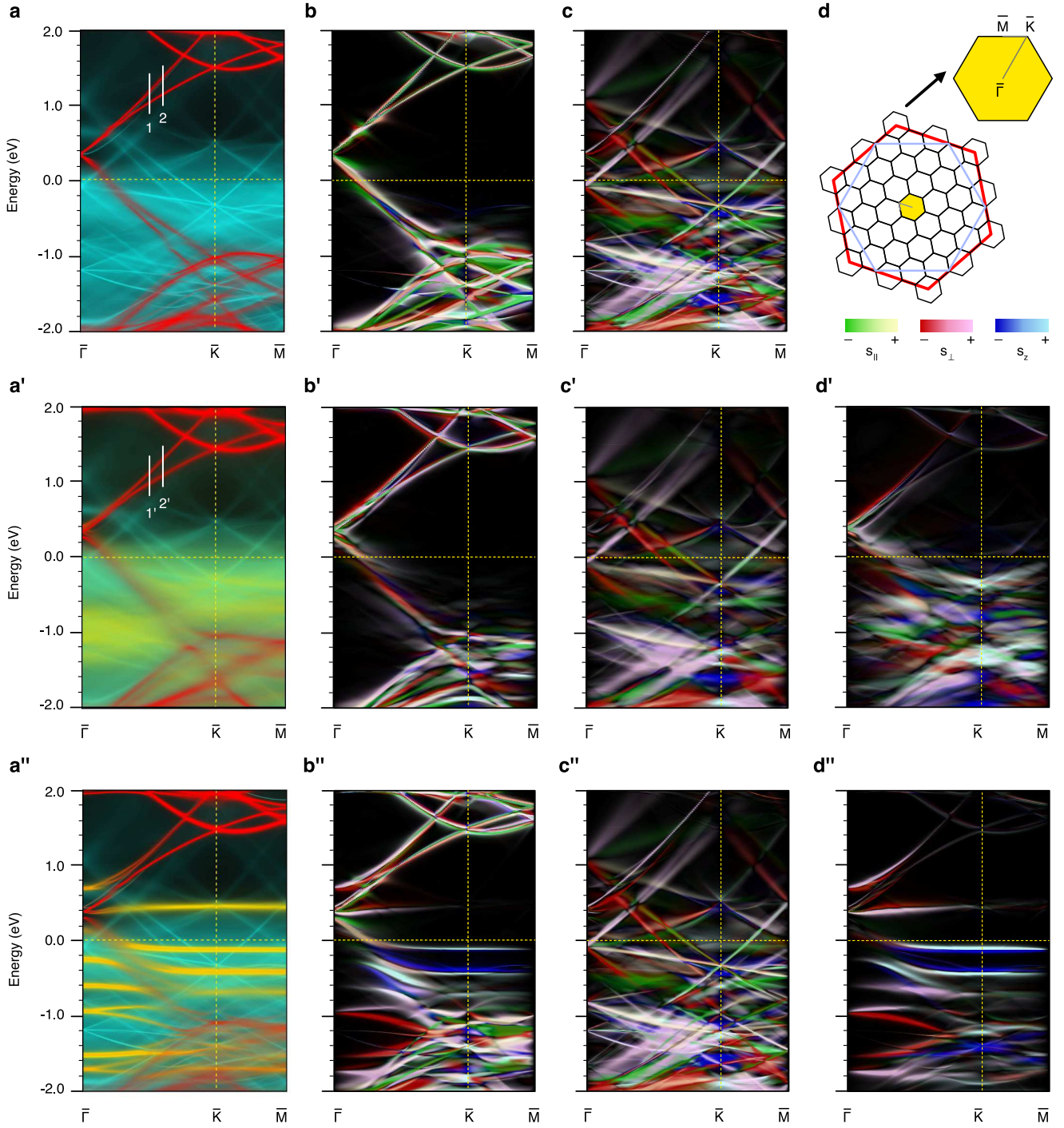


FIG. 2. Electronic and spin structure of G/Pt(111) intercalated/decorated with single Pt atoms. (a) Density of states of G/Pt(111) calculated in (6×6) supercell and projected on graphene (red) and Pt (light-blue). (b) Corresponding spin texture projected on graphene. The color scheme is defined as follows: green/red shades refer to the direction of spin parallel/perpendicular to the momentum, while blue corresponds to the out-of-plane component; light/dark tones denotes positive/negative values of each component, see also the inset summarizing the legends in the bottom of panel (d). (c) Same as (b) projected on Pt substrate. (d) Brillouin zones of the (6×6) supercell (small black hexagons), G- (1×1) primitive cell (red hexagon), and Pt- (1×1) primitive cell (blue hexagon). The selected k -lines are marked within the yellow hexagon in the center. (a'-c') Same as (a-c) for the configuration with intercalated Pt atom; its PDOS in (a') is colored in yellow, and its spin texture is displayed in (d'). (a''-d'') Same as (a'-d') for configuration with single Pt atoms adsorbed on top of G.

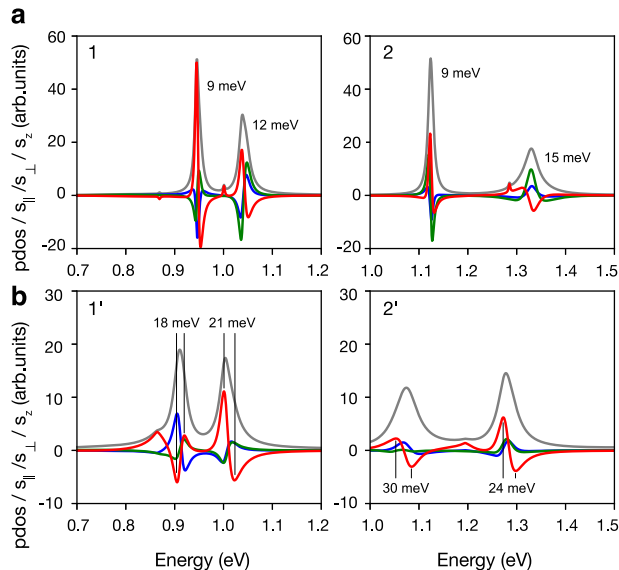


FIG. 3. PDOS(E) and $\bar{s}(E)$ single spectra extracted from the maps in Fig.2 (a)-(a') at two different k -points (left-hand and right-hand panels) marked with white lines in Fig.2. Panel (a) corresponds to the defect free case and (b) to the intercalated model. Only unoccupied DC branches are shown. The numbers shown in the plots refer to the values of spin-orbit derived spin-splitting of the bands corresponding to each peak in PDOS(E). Grey, red, green and blue lines represent the PDOS, and s_{\perp} , s_{\parallel} and s_z components, respectively.

quasi-atomic states at energies around -0.1 , -0.4 and -0.6 eV can be clearly seen in the G-projected (\vec{k}, E) map throughout the entire BZ due to their strong hybridization; they present a spin splitting of ~ 200 meV and as they tear the DCs, the π -bands are endowed with similar splittings. At each anti-crossing region their magnetization aligns with that of the Pt_{ad} state (of intrinsic character) and maintain this orientation (mainly out-of-plane, $\pm s_z$) until the next anti-crossing. The Pt surface, nevertheless, still influences the G's spin texture, specially at energies where the Pt_{ad} bands are absent: below -1 eV and above $+1$ eV, where the in-plane s_{\perp} and s_{\parallel} spin components become patent.

C. Dirac point analysis

In Figure 4 we present high resolution graphene projected PDOS and s_{\parallel} and s_{\perp} (\vec{k}, E) maps around the Dirac point (DP) for the three configurations considered; the s_z component has been omitted since it is significantly less intense than the in-plane ones in all cases. Additionally, and in order to visualize the role played by the SOC, in the leftmost column we present the graphene's PDOS calculated under the scalar-relativistic approximation. For the defect free case, panel (a), and in the absence of SOC we obtain sharp linear π -bands and a gapless DC con-

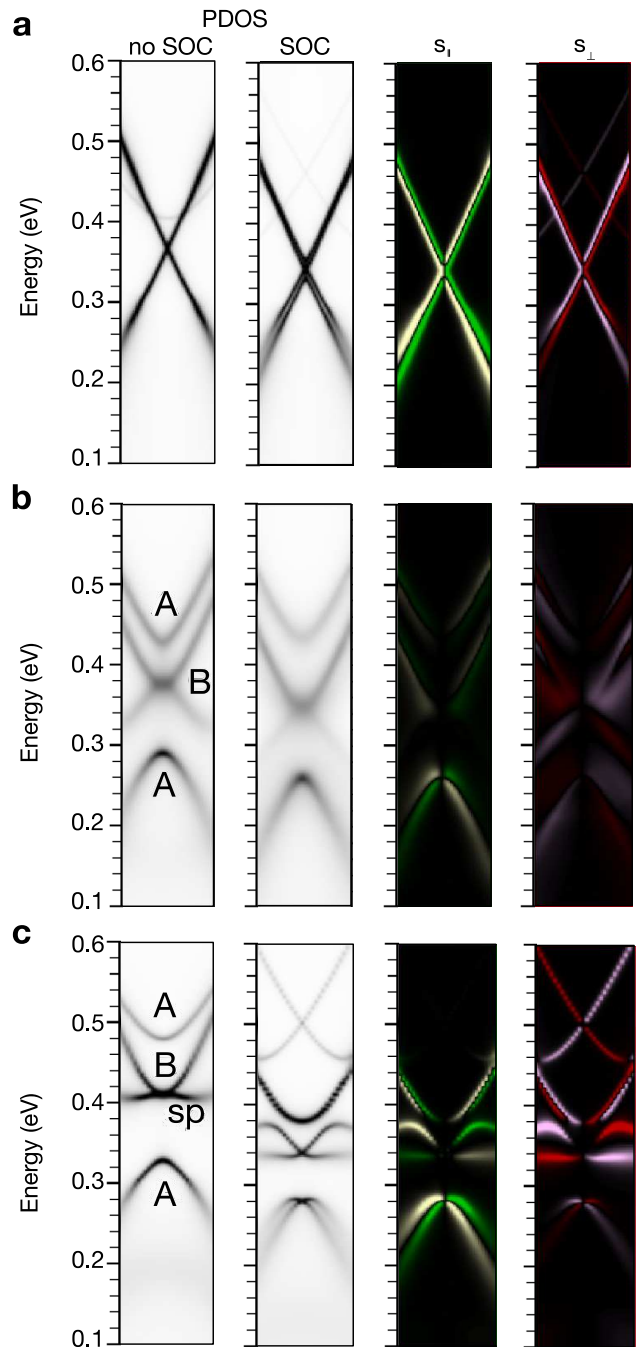


FIG. 4. G-projected electronic and spin structure around the Γ point for the G/Pt(111) systems: (a) defect-free, (b) intercalated Pt_{in} defect and (c) decorated Pt_{ad} defect. First and second columns show the PDOS obtained without and with SOC, respectively, while right-hand columns correspond to the in-plane spin components, s_{\parallel} and s_{\perp} .

sistent with the quasi-free standing character of the G. When the spin-orbit coupling is turned on, the intrinsic SOC opens a small gap (below 10 meV) which, however, is hindered by the broadening of the π -bands due to their hybridization with the Pt substrate. Hence, no quantum

spin Hall phase is expected. On the other hand, Rashba SOC is patent in the $s_{\parallel/\perp}$ maps with splittings of the order of 10 meV (30 meV) in the upper (lower) cones. Furthermore, the spin texture is far from helical, having a larger s_{\parallel} component than s_{\perp} .

The quasi-free standing picture changes drastically for the two defected configurations. In the intercalated case, panel (b), sublattice symmetry is broken since the Pt adatom resides below a C atom (sublattice A), opening a large gap (≈ 130 meV) between its associated DCs, while the other DP (sublattice B) remains gapless, although the bands lose their linear behaviour. Furthermore, the G's PDOS intensity is significantly smaller than in the defect-free case due to the reduced C-Pt distance. The main effect of the SOC here is an increase in the gap for DP-A and of the Rashba splitting of all cones. This is particularly clear in the lower DC-A, where the splittings attain values close to 40 meV. When the Pt adatom is adsorbed on top of a C atom, panel (c), the sublattice symmetry is again broken and a gap larger than 150 meV opens at the DP-A. On the other hand, the lower DC associated to the sublattice B is destroyed due to the presence of the Pt_{ad} sp atomic level at around 0.4 eV. Apart from the Rashba splitting of the lower DC-A (larger than 40 meV) and, to a less extent, of the upper DC-B, SOC induces a splitting of the adatom's sp state, so that one component remains flat (at around 0.34 eV) while the other bends as it anti-crosses the DC.

IV. ADSORPTION OF SINGLE AU ADATOMS IN G/AU/NI(111)

The relaxed geometries for the G/Au/Ni(111) system are shown in Figures 1(d), (e) and (f) for the defect-free case, the intercalated Au_{in} adatom and the adatom Au_{ad} on top of the G, respectively. In the former, the weak G-Au interaction^{10,34-38} leaves an uncorrugated graphene layer lying 3.4 Å above the metal surface. Figures 5(a-c) summarize its associated electronic and spin structure along the high-symmetry lines of the supercell's BZ.¹⁰ Overall, the hybridization between graphene and the underlying Au/Ni(111) is weaker than in G/Pt(111) case. In the combined PDOS(\vec{k}, E) map (a), the G (red), Au (light blue) and Ni surface (dark blue) projections have been superimposed. The quasi-freestanding character of the G manifests in almost undoped and well-preserved DCs down to binding energies of around -1 eV, in agreement with previous experimental works.^{39,40} The most intense Ni related features are located at approximately -0.6 and $+0.1$ eV, corresponding to the top of the majority and minority d -bands, respectively. Several gold sp bands (the most prominent of them the Shockley-type surface state^{30,41} (SS) emerging from Γ at -0.33 eV) cross the BZ whereas fingerprints of the Au $5d$ -bands (light blue) appear below -1 eV distorting the DCs.

In spite of the fact that this system is magnetic and, hence, there exists an interplay between SOC and

exchange interactions, the G's spin texture shown in Fig. 5(b) appears far less complex than in the G/Pt(111) case. Indeed, in the $[-1, +1]$ eV range where the DCs appear almost intact, their spin vector has only two components both perpendicular to the momentum:¹⁰ an in-plane helical component arising solely from the SOC, s_{\perp} , and an out-of-plane one, s_z , mainly induced by the Ni magnetic order. It is also noteworthy the different broadenings of the spin-split branches, particularly around the DP at Γ where the minority (dark blue) component is much broader than the majority one (light blue) whereas along $K - M$ and at around -0.9 eV the opposite behavior holds. The π -band splittings in this energy window are only of the order of 10 meV, in agreement with previous experimental data³⁹ and several theoretical results^{10,11,40}. However, the helical spin texture should not hold anymore when domains with different in-plane magnetizations are present at the Ni surface, as expected in real samples⁴⁰. In such case, one may still expect that the values of the splittings will remain small since their magnitude is mainly related to the magnetic coupling between the G and the Au/Ni(111) surface rather than to the SOC.

The spin projected on the intercalated Au layer (panel (c)), on the other hand, mainly reflects the hybridization with the Ni(111) spin-polarized bands again displaying light (majority) and dark blue (minority) regions. SOC manifests most notably in the lower energy region (below -1.0 eV), where large in-plane components (red) can be clearly seen at several energies.

A. Intercalation with single gold atoms

We again explored the role of adatoms either adsorbed above the graphene or intercalated between the graphene and the Au monolayer. The relaxed structures, shown in Figs. 1(e) and (f), follow analogous trends as in the G/Pt system. The intercalated adatom induces a significant buckling in the G (0.8 Å) while its average distance to the top Au layer is significantly increased from 3.4 Å to 3.9 Å. The associated PDOS and spin (\vec{k}, E) maps are presented in the middle panels in Fig. 5. As shown in (a') where the additional Au_{in} projection is colored in yellow, and in contrast to the G/Pt(111) case, the intercalated adatom introduces only subtle changes in the band structure (e.g. removal of the Au's SS) leaving the graphene's DCs hardly affected. The contribution of the highly delocalized Au_{in} sp states covers most of the map as can be seen by the change in the blue tones compared to the defect-free configuration in panel (a), while intense d -states appear below -1 eV showing little dispersion. We also note that Au_{in} shows no significant spin-polarization (below $0.01 \mu_B$) when intercalated. The spin textures projected on the G and the gold surface layer, panels (b') and (c'), respectively, are very similar to their defect-free counterparts ((b) and (c)), implying that the adatom has little impact on them. The main

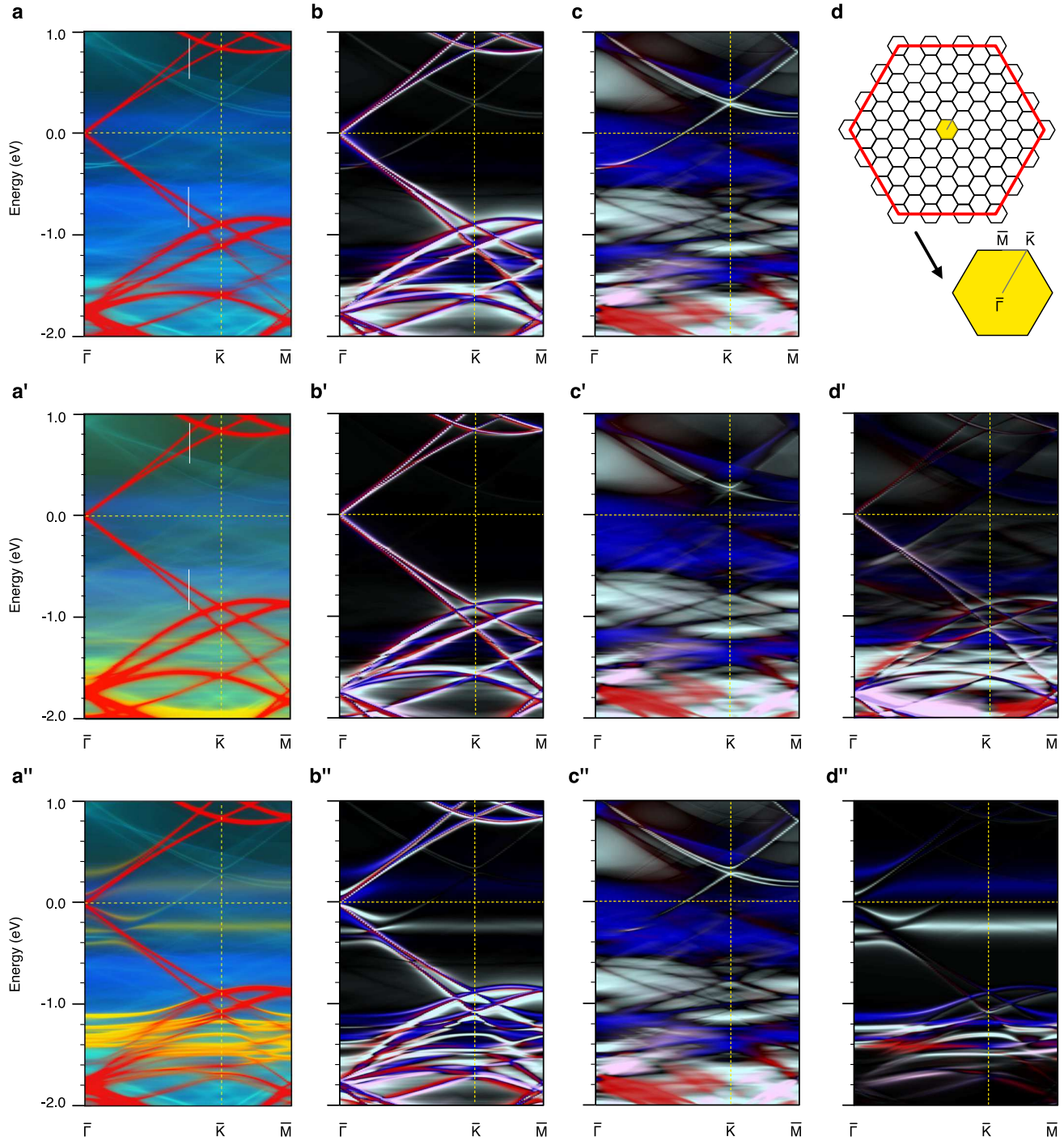


FIG. 5. Electronic and spin structure of G/Au/Ni(111) intercalated/decorated with single Au atoms. (a) Band structure of G/Au/Ni(111) along $\Gamma - K - M$ in folded (9×9) BZ represented as $\text{PDOS}(\vec{k}, E)$ projected on graphene (red), gold (light blue) and Ni surface (dark blue) superimposed at one map. (b) Corresponding graphene's spin texture after superimposing the $x/y/z$ components, each color coded as explained in Fig.2. (c) Same as (b), but projected on intercalated Au layer. (d) Brillouin zones of the (9×9) supercell (small black hexagons), and G- (1×1) primitive cell (red hexagon); the considered k -lines are labeled within the yellow hexagon. (a'-c') Same as (a-c) for the configuration with additional Au atom intercalated below the G; yellow shades in (a') denote its PDOS, while panel (d') shows its spin texture. (a''-d'') Same as (a'-d') for the configuration of G/Au/Ni(111) with Au atoms adsorbed on top of the G. The spin textures projected on Ni(111) are neglected in all cases.

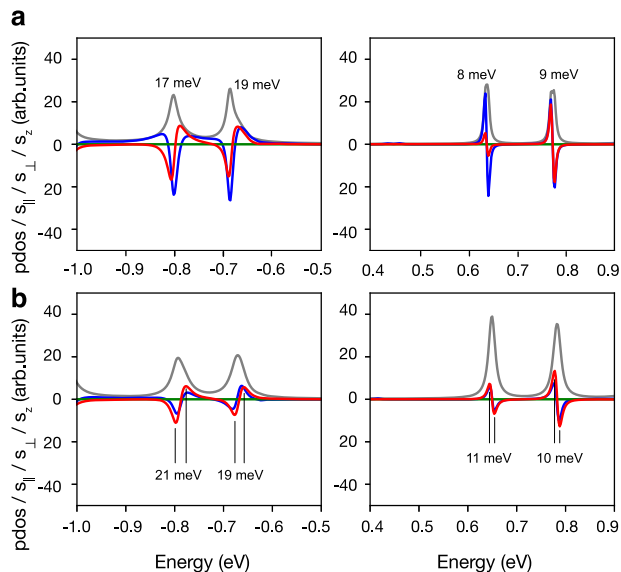


FIG. 6. PDOS(E) and $\vec{s}(E)$ single spectra extracted from the maps in Fig.5 (a)-(a') at specific k -point marked with white lines. Panel (a) corresponds to the defect-free case and (b) to the model containing additional intercalated Au atom. Left-hand (right-hand) panel shows occupied (unoccupied) DC branches. The numbers shown in the plots refer to the values of spin-orbit derived spin-splitting of the bands corresponding to each peak in PDOS(E). Grey, red, green and blue lines represent the PDOS, and s_{\perp} , s_{\parallel} and s_z components, respectively.

difference is a reduction of the π -band broadening due to the enlarged G-Au average distance. In Fig. 6 we compare G-projected DOS(E) and $\vec{s}(E)$ curves between the defect-free (a) and the intercalated (b) cases for both the lower and upper DCs at a representative k -point (marked by the white segments in Figs. 5a-a'). There are only very small changes (a few meV) in the splittings between both systems, with values of ~ 10 meV in the upper cones and ~ 20 meV in the lower ones. Therefore, intercalation of an Au adatom hardly enhances the SOC derived spin splitting in the G/Au/Ni(111) system, in contrast to the G/Pt(111) case. We assign this difference to the absence of $\text{Au}_{\text{in}}-d$ states close to E_f .

B. Decoration with single gold atoms

When Au_{ad} is adsorbed on top of the G, the latter remains hardly corrugated (0.15 \AA), while the C- Au_{ad} bond distance becomes very short (2.46 \AA). Below -1 eV , the atomic-like $\text{Au}_{\text{ad}} d$ -states (intense yellow in (a'')) strongly hybridize with the DCs opening multiple gaps. Moreover, the most relevant feature is the pair of flat bands that run above and below E_f and which strongly perturb and tear the π -bands close to the DP. As can be clearly seen in the G and Au_{ad} spin projections of panels (b'') and (d''), each band holds opposite spins with only s_z component.

An orbital analysis reveals that they correspond to the $6s$ state of Au_{ad} which is exchange splitted by $\sim 0.4 \text{ eV}$ and, in analogy with an Au isolated atom, is responsible for the adatom's spin polarization (the total Au_{ad} 's magnetic moment is $0.56 \mu_B$). The analogous calculation for the simpler G+ Au_{ad} model (that is, after removing the Au/Ni(111) surface), shown in Figure 9, yields a very similar band and spin structure, indicating that the spin polarization of the Au_{ad} atom is unrelated to that of the substrate. This is further corroborated by the fact that the spin texture projected on the Au layer (c'') is almost identical to that of the defect-free case (c).

C. Dirac point analysis

High-resolution graphene projected PDOS and s_{\perp} and $s_z(\vec{k}, E)$ maps are displayed in Figure 7 for the three G/Au/Ni(111) configurations (this time the s_{\parallel} component is negligible in all cases). The equivalent PDOS and s_z maps calculated neglecting SOC have been omitted since they are visually identical to those shown in the figure. Therefore, as stated above, the role of SOC in this system is mainly to introduce an s_{\perp} spin component (helical spin texture). Similar to the G/Pt case, the defect-free configuration presents quasi-perfect DCs while the possible presence of a small gap due to intrinsic SOC is masked by the broadening of the π -bands. The broadening, in fact, is much larger for the $-s_z$ bands (dark), as could be expected from the fact that the Au/Ni(111) PDOS around the Fermi level is mainly occupied by the minority Ni bands.

As shown in panel (b), intercalation of Au_{in} hardly alters the DP or its spin texture due to the low Au PDOS around the E_f (the adatom's d -states all lie at binding energies below -1 eV). However, the situation is drastically different when the G is decorated by the adatom (panel (c)). The interaction between the spin-splitting $\text{Au}_{\text{ad}} s$ -levels induces a large gap in the DCs associated to sublattice A (the C atom below Au_{ad}) which are also spin-splitting (bright and dark parabolas in the s_z map). In contrast, the DCs of the sublattice B remain fairly linear except for a small gap at Γ .

V. SUMMARY AND CONCLUSIONS

We have investigated the spin-orbit proximity effect in graphene on metallic substrates decorated or intercalated by metallic adatoms focusing on two specific graphene/metal systems, non-magnetic G/Pt(111) and magnetic G/Au/Ni(111) previously studied experimentally.^{12,39,40,42,43} Depending on the location of the adatom, two very different scenarios are reached; adsorption on top leaves the graphene essentially uncorrugated but hybridizations with the atomic-like d -states leads to densely teared π bands resembling freestanding graphene decorated by adatoms. It turns out that in

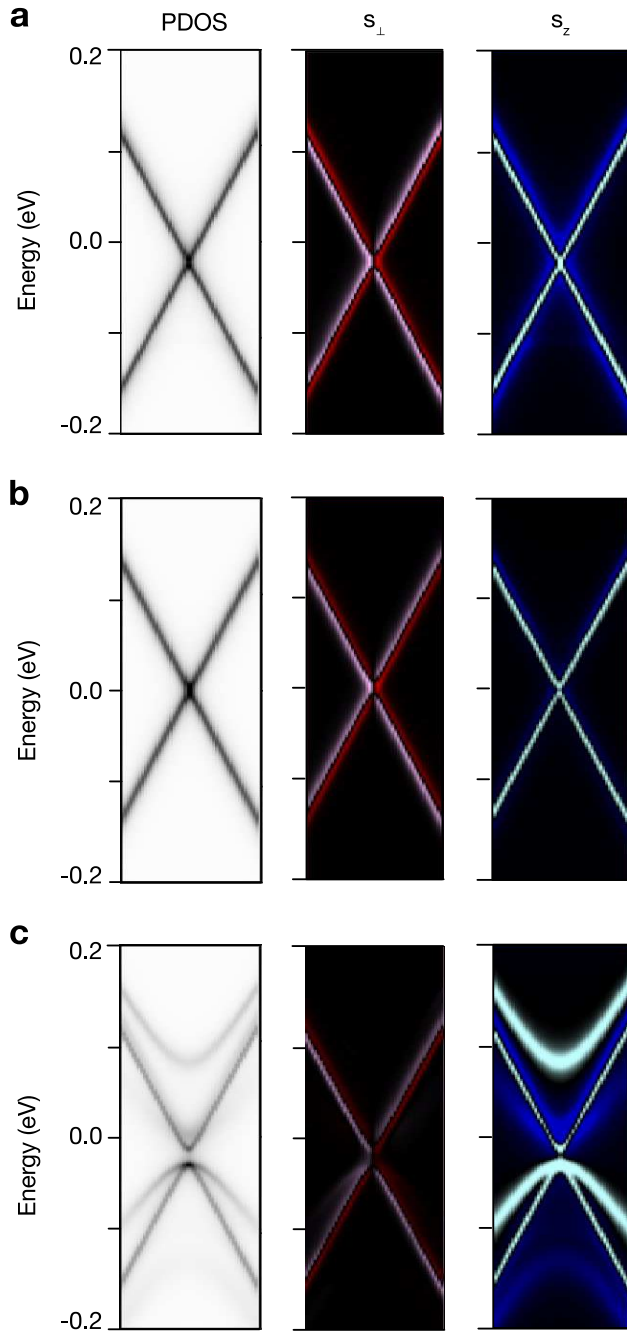


FIG. 7. G-projected electronic and spin structure around the Γ point for the G/Au/Ni(111) systems: (a) defect-free, (b) intercalated Au_{in} defect and (c) decorated Au_{ad} defect. Left, center and right columns show the PDOS, as well as the s_{\perp} and s_z spin components, respectively.

the two systems considered the Pt_{ad} and Au_{ad} adatoms present states close to E_f , thus the quasi-linear parts of the DCs close to the DP are largely distorted and the electronic structure of G loses its linear character.

On the other hand, when intercalated between the

graphene and the metal surface the former becomes highly corrugated making short bonds with the adatom but with an average distance to the surface larger (by ~ 0.4 Å) than in the defect-free case. In this geometry, the adatom's states strongly hybridize with the substrate's continuum of bands largely losing their atomic-like character and therefore, their effect on the π -bands is less intense than for adsorption on top. In G/Pt(111) the upper DCs remain almost unaltered exhibiting a SOC-induced complex spin texture similar to the defect-free case. Interestingly, the close proximity of the G to the Pt_{in} leads to an increase in the π -band splittings in the empty states region by up to a factor of three. This is not the case, however, for G/Au/Ni(111) which presents similar splittings as in the defect-free case since the Au_{in} d -states lie at higher binding energies and their impact on the upper DC is less significant.

A detailed analysis of the G's Dirac point shows that the role of intrinsic SOC is minimal in all configurations, inducing gaps smaller than the broadening of the π -bands; this is an expected result since in all the defected configurations the G's sublattice symmetry is broken.⁴ Therefore, the proximity effect in the systems under consideration relies mainly on the Rashba-type SOC transfer.

Finally, we recall that the G/Au/Ni(111) system is the most puzzling one, since two very different spin-splittings for the π -bands have been reported: around 10 meV³⁹ and giant values close to 100 meV⁴⁰. A subsequent STM study¹², including simplified theoretical models, tentatively assigned the small splittings to a full gold monolayer, while the giant values would correspond to sub-monolayer phases where small Au clusters or even individual atoms lie intercalated between the Ni(111) surface and the G. Furthermore, the Ni surfacemost layer was shown to be reconstructed presenting a misfit dislocation loop structure.⁴⁴ All our models considered, based on a full gold monolayer (plus an adatom), and even taking into account the reconstructed Ni(111) surface¹⁰, always yield small splittings of the order of 10 meV which are driven by the substrate's spin polarization. Therefore, even if the giant splittings come from gold sub-monolayer phases or a different type of Ni-Au surface alloying (which we have not considered), we believe their magnitudes are determined by the magnetic coupling with the metal surface and not by the SOC.

ACKNOWLEDGMENTS

J.S. acknowledges Polish Ministry of Science and Higher Education for the Mobility Plus Fellowship (Grant No. 910/MOB/2012/0). J.I.C acknowledges support from the Spanish Ministry of Economy and Competitiveness under contract Nos. MAT2015-66888-C3-1R and RTI2018-097895-C41. Part of the calculations have been done using the supercomputer facilities at the Barcelona Supercomputing Center under the activity ID QCM-2015-2-0008.

- ¹ W. Han, R. K. Kawakami, M. Gmitra, and J. Fabian, *Nature Nanotech.* **9**, 794 (2014).
- ² A. Avsar, J. Y. Tan, T. Taychatanapat, J. Balakrishnan, G. Koon, Y. Yeo, J. Lahiri, A. Carvalho, A. S. Rodin, E. O-Farrell, G. Eda, A. H. C. Neto, and B. Ozyilmaz, *Nat. Commun.* **5**, 4875 (2014).
- ³ S. Irmer, T. Frank, S. Putz, M. Gmitra, D. Kochan, and J. Fabian, *Phys. Rev. B* **91**, 115141 (2015).
- ⁴ C. Weeks, J. Hu, J. Alicea, M. Franz, and R. Wu, *Phys. Rev. X* **1**, 021001 (2011).
- ⁵ M. Gmitra and J. Fabian, *Phys. Rev. B* **92**, 155403 (2015).
- ⁶ A. M. Shikin, A. G. Rybkin, D. Marchenko, A. A. Rybkina, M. R. Scholz, O. Rader, and A. Varykhalov, *New Journal of Physics* **15**, 013016 (2013).
- ⁷ Z. Y. Li, Z. Q. Yang, S. Qiao, J. Hu, and R. Q. Wu, *Journal of Physics: Condensed Matter* **23**, 225502 (2011).
- ⁸ J. Balakrishnan, G. K. W. Koon, A. Avsar, Y. Ho, J. H. Lee, M. Jaiswal, S.-J. Baeck, J.-H. Ahn, A. Ferreira, M. A. Cazalilla, A. H. C. Neto, and B. Ozyilmaz, *Nat. Commun.* **5**, 4748 (2014).
- ⁹ D. Ma, Z. Li, and Z. Yang, *Carbon* **50**, 297 (2012).
- ¹⁰ J. Sławińska and J. I. Cerdá, *Phys. Rev. B* **98**, 075436 (2018).
- ¹¹ E. Voloshina and Y. Dedkov, *Advanced Theory and Simulations* **1**, 1800063 (2018).
- ¹² M. Krivenkov, E. Golias, D. Marchenko, J. Sánchez-Barriga, G. Bihlmayer, O. Rader, and A. Varykhalov, *2D Materials* **4**, 035010 (2017).
- ¹³ F. Calleja, H. Ochoa, M. Garnica, S. Barja, J. J. Navarro, A. Black, M. M. Otrokov, E. V. Chulkov, A. Arnau, A. L. Vazquez de Parga, F. Guinea, and R. Miranda, *Nature Phys.* **11**, 43 (2015).
- ¹⁴ S. Woo, S. Hemmatiyani, T. D. Morrison, K. D. D. Rathnayaka, I. F. Lyuksyutov, and D. G. Naugle, *Applied Physics Letters* **111**, 263502 (2017).
- ¹⁵ K. Pi, K. M. McCreary, W. Bao, W. Han, Y. F. Chiang, Y. Li, S.-W. Tsai, C. N. Lau, and R. K. Kawakami, *Phys. Rev. B* **80**, 075406 (2009).
- ¹⁶ K. M. McCreary, K. Pi, A. G. Swartz, W. Han, W. Bao, C. N. Lau, F. Guinea, M. I. Katsnelson, and R. K. Kawakami, *Phys. Rev. B* **81**, 115453 (2010).
- ¹⁷ J. Ren, H. Guo, J. Pan, Y. Y. Zhang, X. Wu, H.-G. Luo, S. Du, S. T. Pantelides, and H.-J. Gao, *Nano Letters* **14**, 4011 (2014).
- ¹⁸ M. Petrovic, I. Srut Rakic, S. Runte, C. Busse, J. T. Sadowski, P. Lazic, I. Pletikovic, Z.-H. Pan, M. Milun, P. Pervan, N. Atodiresei, R. Brako, D. Sokcevic, T. Valla, T. Michely, and M. Kralj, *Nature Communications* **4**, 2772 EP (2013).
- ¹⁹ P. Zhao, P. Ren, C. J. K.-J. Weststrate, Y. Xu, D.-B. Cao, H. Xiang, J. Xu, Y. Yang, Y.-W. Li, J. W. H. Niemantsverdriet, X. Wen, and X. Yu, *The Journal of Physical Chemistry C* **122**, 22903 (2018).
- ²⁰ S. Ichinokura, K. Sugawara, A. Takayama, T. Takahashi, and S. Hasegawa, *ACS Nano* **10**, 2761 (2016).
- ²¹ I. I. Klimovskikh, M. M. Otrokov, V. Y. Voroshnin, D. Sostina, L. Petaccia, G. Di Santo, S. Thakur, E. V. Chulkov, and A. M. Shikin, *ACS Nano* **11**, 368 (2017).
- ²² M. M. Otrokov, I. I. Klimovskikh, F. Calleja, A. M. Shikin, O. Vilkov, A. G. Rybkin, D. Estyunin, S. Muff, J. H. Dil, A. L. V. de Parga, R. Miranda, H. Ochoa, F. Guinea, J. I. Cerdá, E. V. Chulkov, and A. Arnau, *2D Materials* **5**, 035029 (2018).
- ²³ J. Brede, J. Sławińska, M. Abadia, C. Rogero, J. E. Ortega, I. Piquero-Zulaica, J. Lobo-Checa, A. Arnau, and J. I. Cerdá, *2D Materials* **4**, 015016 (2017).
- ²⁴ M. Kralj, *Nature Physics* **11**, 11 (2014).
- ²⁵ J. M. Soler, E. Artacho, J. D. Gale, A. Garcia, J. Junquera, P. Ordejon, and D. Sanchez-Portal, *Journal of Physics: Condensed Matter* **14**, 2745 (2002).
- ²⁶ J. Cerdá, M. A. Van Hove, P. Sautet, and M. Salmeron, *Phys. Rev. B* **56**, 15885 (1997).
- ²⁷ E. T. R. Rossen, C. F. J. Flipse, and J. I. Cerdá, *Phys. Rev. B* **87**, 235412 (2013).
- ²⁸ J. P. Perdew, K. Burke, and M. Ernzerhof, *Phys. Rev. Lett.* **77**, 3865 (1996).
- ²⁹ F. Ortman, F. Bechstedt, and W. G. Schmidt, *Phys. Rev. B* **73**, 205101 (2006).
- ³⁰ R. Cuadrado and J. I. Cerdá, *Journal of Physics: Condensed Matter* **24**, 086005 (2012).
- ³¹ P. Merino, M. Svec, A. L. Pinardi, G. Otero, and J. A. Martin-Gago, *ACS Nano* **5**, 5627 (2011).
- ³² C. Rogero, J. A. Martin-Gago, and J. I. Cerdá, *Phys. Rev. B* **74**, 121404 (2006).
- ³³ J. Sławińska and I. Zasada, *Phys. Rev. B* **84**, 235445 (2011).
- ³⁴ G. Giovannetti, P. A. Khomyakov, G. Brocks, V. M. Karpan, J. van den Brink, and P. J. Kelly, *Phys. Rev. Lett.* **101**, 026803 (2008).
- ³⁵ Z. Klusek, P. Dabrowski, P. Kowalczyk, W. Kozłowski, W. Olejniczak, P. Blake, M. Szybowicz, and T. Runka, *Applied Physics Letters* **95**, 113114 (2009).
- ³⁶ J. Sławińska, P. Dabrowski, and I. Zasada, *Phys. Rev. B* **83**, 245429 (2011).
- ³⁷ J. Sławińska, I. Wlasny, P. Dabrowski, Z. Klusek, and I. Zasada, *Phys. Rev. B* **85**, 235430 (2012).
- ³⁸ T. Olsin and K. S. Thygesen, *Phys. Rev. B* **87**, 075111 (2013).
- ³⁹ A. Varykhalov, J. Sanchez-Barriga, A. M. Shikin, C. Biswas, E. Vescovo, A. Rybkin, D. Marchenko, and O. Rader, *Phys. Rev. Lett.* **101**, 157601 (2008).
- ⁴⁰ D. Marchenko, A. Varykhalov, M. Scholz, G. Bihlmayer, E. Rashba, A. Rybkin, A. Shikin, and O. Rader, *Nat Commun* **3**, 1232 (2012).
- ⁴¹ S. LaShell, B. A. McDougall, and E. Jensen, *Phys. Rev. Lett.* **77**, 3419 (1996).
- ⁴² A. M. Shikin, A. A. Rybkina, A. G. Rybkin, I. I. Klimovskikh, P. N. Skirdkov, K. A. Zvezdin, and A. K. Zvezdin, *Applied Physics Letters* **105**, 042407 (2014).
- ⁴³ I. I. Klimovskikh, S. S. Tsirkin, A. G. Rybkin, A. A. Rybkina, M. V. Filianina, E. V. Zhizhin, E. V. Chulkov, and A. M. Shikin, *Phys. Rev. B* **90**, 235431 (2014).
- ⁴⁴ J. Jacobsen, L. Pleth Nielsen, F. Besenbacher, I. Stensgaard, E. Laegsgaard, T. Rasmussen, K. W. Jacobsen, and J. K. Nørskov, *Phys. Rev. Lett.* **75**, 489 (1995).
- ⁴⁵ S. Kunschuh, M. Gmitra, and J. Fabian, *Phys. Rev. B* **82**, 245412 (2010).
- ⁴⁶ T. Frank, S. Irmer, M. Gmitra, D. Kochan, and J. Fabian, *Phys. Rev. B* **95**, 035402 (2017).
- ⁴⁷ S. Abdelouahed, A. Ernst, J. Henk, I. Maznichenko, and I. Mertig, *Phys. Rev. B* **82**, 125424 (2010).

Appendix A: Graphene decorated by single metal adatoms

Although pure decoration of graphene with single metal adatoms was widely studied in the literature and is well understood in terms of model Hamiltonians,^{45–47} we present below DFT calculations without the substrates employing the same supercells as considered for the systems discussed in the main text. Figures 8 and 9 show the electronic and spin properties of graphene decorated by a single Pt and Au atom, respectively, without including any metallic surface.^{9,13,40,47} In both cases, the overall picture is similar to the analogous configuration on top of the metallic substrate, which confirms that the graphene-adatom interaction becomes dominant. We can easily observe in Fig. 8 that the states of the adatom strongly interact with the DCs opening a ~ 100 meV band gap and several anticrossing gaps below E_F . Comparing with Fig.2 (a''), we can conclude that the only effect of the metallic substrate is the p -type doping of ~ 300 meV and the broadening of the bands due to the interaction with several substrate's states. In the case of G/Au/Ni system (Fig. 9) the interaction between graphene and Au adatom induces similar changes in the DCs, but given the smaller number of Au states close to the Fermi level, the

DCs are less perturbed than in case of the decoration with Pt atom. From comparison with Fig. 5 (a'') it is clear that the substrate plays hardly any role; this behavior is quite expected as graphene can be considered quasi-freestanding on Au/Ni.

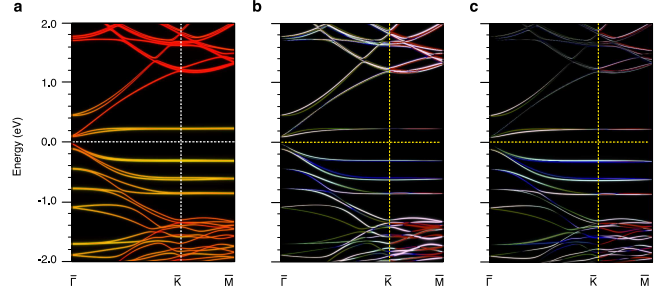


FIG. 8. (a) $\text{DOS}(\vec{k}, E)$ map projected on the G (red) and Pt adatom (yellow). No substrate was included in this case. (b) Spin texture corresponding to graphene's PDOS presented in (a). (c) Same as (b) projected on Pt adatom. Color scheme same as in Figs 2 and 5.

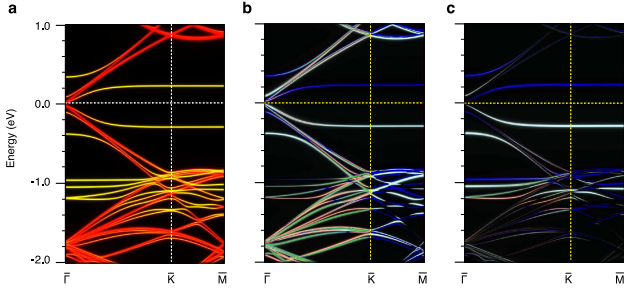


FIG. 9. (a) $\text{DOS}(\vec{k}, E)$ map projected on the G (red) and Au adatom (yellow). No substrate was included in this case. (b) Spin texture corresponding to graphene's PDOS presented in (a). (c) Same as (b) projected on Au adatom. Color scheme same as in Figs 2 and 5.